

**Dynamical thermalization in Bose-Hubbard systems**Peter Schlagheck<sup>1</sup> and Dima L. Shepelyansky<sup>2</sup><sup>1</sup>*Département de Physique, University of Liege, 4000 Liège, Belgium*<sup>2</sup>*Laboratoire de Physique Théorique, CNRS, IRSAMC, Université de Toulouse, UPS, 31062 Toulouse, France*

(Received 7 October 2015; revised manuscript received 17 December 2015; published 19 January 2016)

We numerically study a Bose-Hubbard ring of finite size with disorder containing a finite number of bosons that are subject to an on-site two-body interaction. Our results show that moderate interactions induce dynamical thermalization in this isolated system. In this regime the individual many-body eigenstates are well described by the standard thermal Bose-Einstein distribution for well-defined values of the temperature and the chemical potential, which depend on the eigenstate under consideration. We show that the dynamical thermalization conjecture works well at both positive and negative temperatures. The relations to quantum chaos, quantum ergodicity, and the Åberg criterion are also discussed.

DOI: [10.1103/PhysRevE.93.012126](https://doi.org/10.1103/PhysRevE.93.012126)**I. INTRODUCTION**

A quantum system that is in contact with a thermostat is described by the well-known quantum thermal distributions given in textbooks on statistical physics (see, e.g., Ref. [1]). However, there has always been an interest (raised, e.g., in the works of Bohr on the statistical description of neutron capture and nuclei construction [2]) to understand the emergence of thermalization effects within a complex quantum system through the dynamical properties of the system itself, without the explicit introduction of a thermostat. That is, while the full quantum system is prepared, say, within a pure eigenstate of its Hamiltonian and is therefore not subject to thermalization, the one-body observables of interest in relation to its single-particle eigenstates may nevertheless feature the standard thermodynamic properties known from textbook statistical physics as a consequence of the presence of interactions within the system.

Of course, the emergence of such a statistical description in the absence of any thermostat, which we call the dynamical thermalization conjecture (DTC) in the following, requires quantum ergodicity of the system eigenstates. Research on this latter topic has been stimulated by the works of Åberg [3,4], as well as by Deutsch [5] and Srednicki [6], which generated a broad discussion of the eigenstate thermalization hypothesis (ETH) as well as various investigations of different research groups (see the references and the discussion in Ref. [7] and in the recent review in [8]).

It is clear that dynamical thermalization is based on quantum ergodicity of eigenstates. In the single-particle context, a mathematical proof of quantum ergodicity was obtained by Shnirelman for eigenstates of one-particle chaotic billiards in the limit of large quantum numbers [9], where the class of billiards with chaotic classical dynamics had previously been established by Sinai and coworkers (see, e.g., Ref. [10]). In such single-particle systems it is numerically straightforward to verify that quantum ergodicity implies the emergence of universal random matrix statistics for the energy levels of the system, which is known as the Bohigas-Giannoni-Schmit conjecture established first for quantum chaos billiards [11]. Thus the development of the field of quantum chaos [12,13] established links between quantum systems with classical dynamical chaos and random matrix theory (RMT) invented

by Wigner for spectra of complex nuclei [14], and it was recognized that the emergence of Wigner-Dyson statistics for energy level spacings is a necessary condition for quantum ergodicity of eigenstates.

However, in spite of significant progress in the field of quantum chaos, studies in this context were mainly related to one-particle systems with a few degrees of freedom [12,13]. Indeed, the properties of many-body quantum systems, e.g., nuclei [15], were hardly accessible to computer simulations at the time of the 1970s and 1980s. At that time the common lore within the nuclear physics community was that in many-body quantum systems the density of states is exponentially growing with the excitation energy above the Fermi level and hence any small interaction between fermions will very rapidly lead to the mixing of noninteracting many-body states accompanied by the RMT statistics of the level spacings, by quantum ergodicity of states, and hence by dynamical thermalization [16]. This lore persisted until the end of the 20th century even though Åberg presented in 1990 numerical and analytical arguments according to which the onset of RMT level spacing statistics, and hence quantum ergodicity, takes place only when directly coupled states are mixed by two-body interactions (which, from a fundamental point of view, are the only ones that exist in nature) [3,4]. The Åberg criterion for the onset of quantum chaos in a weakly interacting many-body system was later confirmed in more advanced studies for other quantum systems, such as finite fermionic systems [17,18] and quantum computers of interacting qubits [19,20], as was reviewed in Ref. [21]. In the latter context of quantum computers, examples of single eigenstates that are well thermalized by the presence of residual weak interactions between qubits and thus satisfy the DTC are presented in [20], showing that such states are also well described by the Fermi-Dirac thermal distribution. In the framework of complex atoms the quantum ergodicity properties of eigenstates and the emergence of DTC have been discussed in Refs. [22,23], but the interactions in such atoms are relatively strong, and the DTC cannot be straightforwardly verified in real atoms.

In the present work we investigate DTC within the physical context of ultracold bosonic quantum gases that are confined within finite optical lattices. Indeed, the impressive experimental progress in the handling of ultracold atoms and the control of their interactions has renewed and pushed the

interest in DTC and ETH and has stimulated a number of studies on this topic which are reviewed in Ref. [8] (see Ref. [24] for a pioneering theoretical work in this context). On the experimental side, recent investigations with cold bosonic atoms allow us to test the validity of generalized Gibbs ensembles under various experimental conditions [25]. Even a realization of negative temperature distributions is now within reach of cold atom experiments, as was shown in Ref. [26]. The problem of DTC and ETH is now actively investigated with ultracold atoms (see, e.g., Ref. [27]).

We shall specifically consider finite Bose-Hubbard systems with  $L$  sites that contain a finite number  $N$  of bosonic atoms. Our subsystem of interest will be one (in practice arbitrarily selected) eigenstate  $|k\rangle$  of the one-body Hamiltonian describing the kinetic energy and the external potential within the Bose-Hubbard lattice (with  $k \in \{1, \dots, L\}$ ). The main message that we want to convey here is that the presence of a thermal reservoir is not necessarily required in order to achieve dynamical thermalization and thereby obtain the Bose-Einstein distribution within such a single-particle eigenstate. We show that a moderate (not too strong and not too weak) two-body interaction  $\hat{U}$ , which couples the single-particle eigenstates with each other, can do this job as well, leading to a thermal description of eigenstates. In that case, the other single-particle states  $|k'\rangle$  with  $k' \neq k$  form an effective “reservoir” for the (sub-)“system” constituted by the single state  $|k\rangle$ . The temperature and the chemical potential that this reservoir provides depend then on the specific state of the global Bose-Hubbard system spanned by the single-particle states  $|k\rangle$ , which can undergo a dynamical process or be prepared in one of the many-particle eigenstates  $|\Phi\rangle$  of the full Bose-Hubbard Hamiltonian. This latter possibility implies that a many-particle eigenstate  $|\Phi\rangle$  of an interacting bosonic Hamiltonian can exhibit grand canonical thermalization features for any single-particle eigenstate  $|k\rangle$  of its one-body (kinetic-plus-potential) part, with an effective temperature  $T$  and an effective chemical potential  $\mu$  that are specific to the state  $|\Phi\rangle$ .

The concept of dynamical thermalization is concretized in some more detail in Sec. II, where we describe the Bose-Hubbard model under consideration. Section III is devoted to presenting and discussing the numerical results that are obtained within this Bose-Hubbard model concerning the DTC. Finally, possible implications of the DTC for a wider class of many-body systems are briefly discussed in Sec. IV.

## II. DYNAMICAL THERMALIZATION WITHIN A BOSE-HUBBARD MODEL

As in Ref. [28], we consider a one-dimensional Bose-Hubbard ring containing  $L$  sites. The quantum many-body Hamiltonian of this system reads  $\hat{H} = \hat{H}_0 + \hat{U}$ , with

$$\hat{H}_0 = -J \sum_{l=1}^L (\hat{a}_l^\dagger \hat{a}_{l-1} + \hat{a}_{l-1}^\dagger \hat{a}_l) + \sum_{l=1}^L \epsilon_l \hat{a}_l^\dagger \hat{a}_l, \quad (1)$$

$$\hat{U} = \frac{U}{2} \sum_{l=1}^L \hat{a}_l^\dagger \hat{a}_l^\dagger \hat{a}_l \hat{a}_l, \quad (2)$$

where  $\hat{a}_l^\dagger$  and  $\hat{a}_l$  respectively denote the creation and annihilation operators associated with site  $l$  and where we formally identify  $\hat{a}_0 \equiv \hat{a}_L$  and  $\hat{a}_0^\dagger \equiv \hat{a}_L^\dagger$ . The on-site energies  $\epsilon_l$  ( $l = 1, \dots, L$ ) are fixed but randomly selected with uniform probability density from the interval  $-W/2 \leq \epsilon_l \leq W/2$ . Evidently, the single-particle Hilbert space of this finite system is  $L$ -dimensional, and the diagonalization of the single-particle Hamiltonian corresponding to  $\hat{H}_0$  therefore yields  $L$  orthogonal and normalized eigenstates  $|0\rangle, |1\rangle, \dots, |L-1\rangle$  satisfying  $\langle k|k'\rangle = \delta_{kk'}$  for all  $k, k' = 0, \dots, L-1$ . The associated eigenenergies  $E_k$  are supposed to be sorted such that we have  $E_0 < E_1 < \dots < E_{L-1}$ .

Introducing the coefficients  $C_{k,l}$  that handle the transformation from the original on-site basis to the single-particle eigenbasis through the relation

$$\hat{a}_l = \sum_{k=0}^{L-1} C_{k,l} \hat{b}_k \quad (3)$$

for all  $l = 1, \dots, L$ , we can now represent the many-body Hamiltonian of the Bose-Hubbard system according to  $\hat{H} = \hat{H}_0 + \hat{U}$ , with

$$\hat{H}_0 = \sum_{k=0}^{L-1} E_k \hat{b}_k^\dagger \hat{b}_k, \quad (4)$$

$$\hat{U} = \frac{U}{2} \sum_{k_1=0}^{L-1} \sum_{k_2=0}^{L-1} \sum_{k_3=0}^{L-1} \sum_{k_4=0}^{L-1} \sum_{l=1}^L C_{k_1,l}^* C_{k_2,l}^* C_{k_3,l} C_{k_4,l} \times \hat{b}_{k_1}^\dagger \hat{b}_{k_2}^\dagger \hat{b}_{k_3} \hat{b}_{k_4}. \quad (5)$$

In the absence of interaction, i.e., for  $U = 0$ , we thereby recover the Hamiltonian (4) whose many-particle eigenstates are given by the Fock states  $|n_0, \dots, n_{L-1}\rangle$  that are defined with respect to the single-particle basis  $(|0\rangle, \dots, |L-1\rangle)$ . Diagonalizing the interacting Hamiltonian  $\hat{H}$  in this representation yields the many-body eigenstates

$$|\Phi_\alpha\rangle = \sum_{n_0=0}^{\infty} \dots \sum_{n_{L-1}=0}^{\infty} C_{n_0, \dots, n_{L-1}}^{(\alpha)} |n_0, \dots, n_{L-1}\rangle, \quad (6)$$

where the coefficients  $C_{n_0, \dots, n_{L-1}}^{(\alpha)}$  reflect the conservation of the total number of particles (i.e., we have  $C_{n_0, \dots, n_{L-1}}^{(\alpha)} = 0$  if  $n_0 + \dots + n_{L-1} \neq N^{(\alpha)}$ , with  $N^{(\alpha)}$  being the total number of particles in the state  $|\Phi_\alpha\rangle$ ). We suppose that these eigenstates are ordered according to their associated eigenenergies  $\mathcal{E}_\alpha$ ; that is, we have  $\mathcal{E}_0 < \mathcal{E}_1 < \mathcal{E}_2 < \dots$ . The representation (6) allows us now to straightforwardly extract the mean population of the single-particle eigenstate  $|k\rangle$  within the many-body state  $|\Phi_\alpha\rangle$  according to

$$\begin{aligned} \langle \hat{n}_k \rangle_\alpha &= \langle \Phi_\alpha | \hat{b}_k^\dagger \hat{b}_k | \Phi_\alpha \rangle \\ &= \sum_{n_0=0}^{\infty} \dots \sum_{n_{L-1}=0}^{\infty} n_k |C_{n_0, \dots, n_{L-1}}^{(\alpha)}|^2. \end{aligned} \quad (7)$$

This mean population can now be compared with the prediction that would result from a quantum statistical modeling in the spirit of the DTC. To this end we effectively treat each single-particle state  $|k\rangle$  as a (sub-)system of interest

and assume that the other states  $|k'\rangle$ , with  $k' \neq k$ , form an effective energy and particle reservoir to which this system is coupled by virtue of the presence of atom-atom interaction. This reservoir is characterized by a given temperature  $T = 1/\beta$  (using temperature units in which  $k_B \equiv 1$ ) and by a given chemical potential  $\mu$ , which both depend on the many-body eigenstate  $|\Phi_\alpha\rangle$  under consideration, i.e.,  $\beta \equiv \beta_\alpha$  and  $\mu \equiv \mu_\alpha$ .

To fully establish the connection with the textbook quantum statistical theory of noninteracting Bose gases [1], we model the dynamics within our system of interest by an effective one-body Hamiltonian of the form  $\hat{H}_k^{(\text{eff})} = \tilde{E}_k \hat{b}_k^\dagger \hat{b}_k$ . While in the absence of interaction we would naturally set  $\tilde{E}_k = E_k$ , the presence of a repulsive (or attractive) atom-atom interaction gives rise to an effective mean-field shift of this energy towards higher (or lower) energies. Assuming that the atoms are more or less equidistributed among the  $L$  sites of the Bose-Hubbard ring for the many-body eigenstate under consideration (which is generally the case in the central part of the many-body spectrum but may not be valid at the upper end of the spectrum in the presence of a repulsive interaction or at the lower end of the spectrum in the presence of an attractive interaction; see also the discussion in the next section), this effective mean-field shift is approximately given by the addition energy  $NU/L$  that would be needed in order to add an extra atom to the interacting system. We therefore set

$$\tilde{E}_k = E_k + NU/L. \quad (8)$$

The statistical density operator of our one-state system is then written as

$$\hat{\rho}_k = \frac{1}{Y_k} \exp[-\beta(\tilde{E}_k - \mu)\hat{b}_k^\dagger \hat{b}_k]. \quad (9)$$

Provided we have

$$\beta(\tilde{E}_k - \mu) > 0, \quad (10)$$

we can express the partition function associated with the eigenstate  $|k\rangle$  as

$$Y_k = \sum_{n=0}^{\infty} e^{-n\beta(\tilde{E}_k - \mu)} = \frac{1}{1 - e^{-\beta(\tilde{E}_k - \mu)}}. \quad (11)$$

It is then straightforward to show that the average population of the single-particle state  $|k\rangle$  is given by the Bose-Einstein distribution

$$\bar{n}_k = \text{Tr}[\hat{\rho}_k \hat{b}_k^\dagger \hat{b}_k] = \frac{1}{e^{\beta(\tilde{E}_k - \mu)} - 1} \equiv \bar{n}_k(\beta, \mu). \quad (12)$$

Applying this reasoning to all single-particle eigenstates of our Bose-Hubbard ring gives us a means to determine the parameters  $\beta$  and  $\mu$  associated with a given many-body eigenstate, provided we can trust the validity of the DTC. Indeed, we must have

$$\sum_{k=0}^{L-1} \bar{n}_k = N \quad (13)$$

due to the conservation of the number of particles, and we can furthermore require that the total energy of the many-body

eigenstate be evaluated as

$$\mathcal{E}_\alpha = \sum_{k=0}^{L-1} \tilde{E}_k \bar{n}_k = \sum_{k=0}^{L-1} E_k \bar{n}_k + N^2 U/L. \quad (14)$$

These two equations can be numerically solved for  $\mu$  and  $\beta$ . For many-body eigenstates with a relatively low total energy  $\mathcal{E}_\alpha$ , we expect to thereby obtain a positive temperature  $T = 1/\beta > 0$  as well as a negative chemical potential satisfying  $\mu < E_k + NU/L$  for all  $k = 0, \dots, L-1$ , in perfect accordance with standard textbook quantum statistical physics [1]. Within the upper part of the spectrum, however, we would have  $\mu > E_k + NU/L$  for all  $k = 0, \dots, L-1$  as well as a negative temperature  $T < 0$ , which appears since the single-particle spectrum of the system is bounded [26]. We note that the concept of negative temperature is well known in spin physics [29], but in our case it has a purely dynamical origin.

### III. NUMERICAL RESULTS

Figure 1 displays the mean populations  $\langle \hat{n}_k \rangle_\alpha$  for various many-body eigenstates that are obtained within a Bose-Hubbard ring of  $L = 8$  sites containing  $N = 8$  particles (yielding a Hilbert space that is spanned by altogether  $\mathcal{N} = 6435$  many-body eigenstates), where we chose the parameters  $U = 0.5J$  and  $W = 4J$ . Each panel of Fig. 1 shows single-particle eigenstate populations for many-body eigenstates. While there are weak fluctuations in the populations, the overall probability distributions appear to remain stable with respect to small variations of  $\alpha$ , which reflects the statistical stability of thermal distributions.

In Fig. 2 we make an averaging of the populations  $\langle \hat{n}_k \rangle_\alpha$  over 20 consecutive many-body eigenstates ranging within  $\alpha_0 - 9 \leq \alpha \leq \alpha_0 + 10$ . After such an averaging, we obtain a qualitative agreement with the general behavior that is expected from the Bose-Einstein distribution (12), shown by

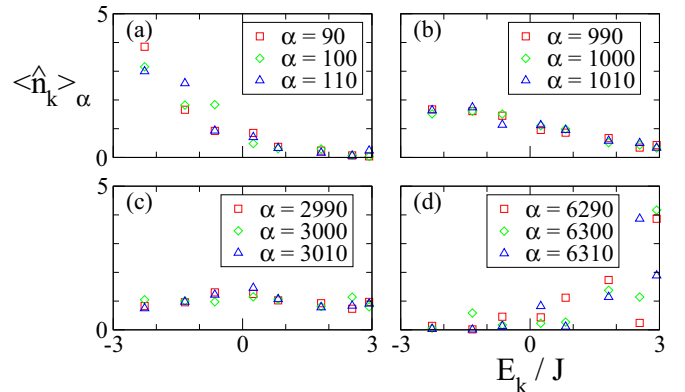


FIG. 1. Distribution of single-particle populations for various many-body eigenstates of the Bose-Hubbard ring with  $N = 8$  particles on  $L = 8$  sites, with the interaction strength  $U = 0.5J$ , and with on-site energies  $\epsilon_i$  that are randomly selected within  $-2J < \epsilon_i < 2J$ . Plotted are the populations  $\langle \hat{n}_k \rangle_\alpha$  as a function of the single-particle levels  $E_k$  ( $k = 0, \dots, 7$ ) for the many-body states  $\alpha$ : (a)  $|\Phi_{90}\rangle, |\Phi_{100}\rangle, |\Phi_{110}\rangle$ , (b)  $|\Phi_{990}\rangle, |\Phi_{1000}\rangle, |\Phi_{1010}\rangle$ , (c)  $|\Phi_{2990}\rangle, |\Phi_{3000}\rangle, |\Phi_{3010}\rangle$ , and (d)  $|\Phi_{6290}\rangle, |\Phi_{6300}\rangle, |\Phi_{6310}\rangle$ .

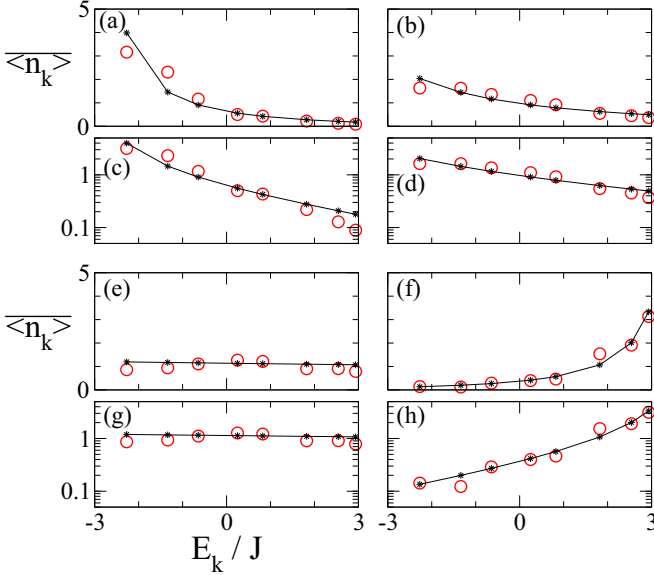


FIG. 2. Average distribution of single-particle populations for the Bose-Hubbard ring with  $N = 8$  particles on  $L = 8$  sites, with the interaction strength  $U = 0.5J$ , and with on-site energies  $\epsilon_l$  that are randomly selected within  $-2J < \epsilon_l < 2J$ . The red circles display, on [(a), (b), (e), and (f)] linear and [(c), (d), (g), and (h)] logarithmic scales, the average populations  $\langle n_k \rangle = 0.05 \sum_{\alpha=\alpha_0-9}^{\alpha_0+10} \langle \hat{n}_k \rangle_\alpha$  for [(a) and (c)]  $\alpha_0 = 100$ , [(b) and (d)]  $\alpha_0 = 1000$ , [(e) and (g)]  $\alpha_0 = 3000$ , and [(f) and (h)]  $\alpha_0 = 6300$ . The stars connected by solid lines show the populations  $\bar{n}_k$  that result from the Bose-Einstein distribution (12), where  $\beta$  and  $\mu$  were chosen such that  $\sum_k \bar{n}_k = N = 8$  and  $\sum_k E_k \bar{n}_k = \sum_k E_k \langle n_k \rangle$ .

solid lines. The agreement of numerical probabilities with the DTC (12) is valid for positive [Figs. 2(a)–2(d)], infinite [Figs. 2(e) and 2(g)], and negative [Figs. 2(f) and 2(h)] temperatures. In the latter case [Figs. 2(f) and 2(h)] the mean population increases with increasing single-particle energy, which, when being compared to Eq. (12), would correspond to a moderately low negative temperature  $T < 0$  and a chemical potential  $\mu > E_{L-1}$ , while a decrease of population with increasing single-particle energy corresponds to the more familiar case of a positive temperature  $T > 0$  and a negative chemical potential  $\mu < E_0$ .

A more detailed comparison of the DTC with the Bose-Einstein distribution (12) is presented in Fig. 3, where we show average single-particle eigenstate populations that are obtained from all many-body eigenstates whose energies lie in given intervals. The agreement between the numerically computed averages (left panels) and the analytical predictions resulting from the Bose-Einstein distribution (12) (right panels) is very good, both on a linear scale and on a logarithmic scale.

To assess the validity of the DTC on a more quantitative level, we extract from the single-particle eigenstate populations (7) effective entropies

$$S_\alpha = - \sum_{k=0}^{L-1} \frac{\langle \hat{n}_k \rangle_\alpha}{N} \ln \left( \frac{\langle \hat{n}_k \rangle_\alpha}{N} \right) \quad (15)$$

that characterize how many single-particle eigenstates are populated within a given many-body eigenstate  $|\Phi_\alpha\rangle$  (and

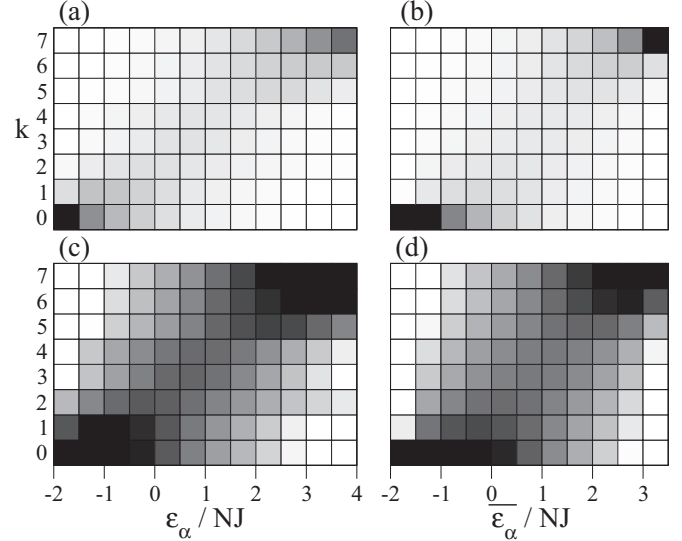


FIG. 3. Left: Average populations of the single-particle eigenstates  $|k\rangle$  as a function of the energy per particle for the Bose-Hubbard ring with  $N = 8$  particles on  $L = 8$  sites, with the interaction strength  $U = 0.5J$ , and with on-site energies  $\epsilon_l$  that are randomly selected within  $-2J < \epsilon_l < 2J$ . The populations are shown on a linear scale in (a) and (b), which uniformly varies from 0 (white) to 8 (black), and on a logarithmic scale in (c) and (d), which uniformly varies from 0.08 (white) to 8 (black). They are averaged over all many-body eigenstates whose energies per particle  $\mathcal{E}_\alpha/N$  lie within the indicated intervals on the abscissa. Right: The corresponding predictions provided by the Bose-Einstein distribution (12), where  $\beta$  and  $\mu$  were chosen such that  $\sum_k \bar{n}_k = N = 8$  and  $\sum_k E_k \bar{n}_k + N^2 U/L = \bar{\mathcal{E}}_\alpha$ , with  $\bar{\mathcal{E}}_\alpha/N$  corresponding to the centers of the abscissa intervals (e.g.,  $\bar{\mathcal{E}}_\alpha/N = -1.75J$  for the leftmost subcolumn of the two panels on the right-hand side).

that are very similar to the one-particle occupation entropies considered in Ref. [30] in the context of many-body localization). Clearly, this entropy will be rather low at the lower and upper edges of the many-body spectrum where only few single-particle states are effectively populated (as is seen in the top left and bottom right panels of Fig. 2, respectively), while it acquires its maximal value  $\ln L$  in the central part of the spectrum where all single-particle eigenstates are equally populated on average. Figure 4 displays  $S_\alpha$  as a function of the energy per particle  $\mathcal{E}_\alpha/N$  for all many-body eigenstates of the Bose-Hubbard ring with  $N = L = 7, 8, 9$  and with the parameters  $W = 4J$  and  $U = \pm 0.5J$ . We see that there is, on average, a remarkable one-to-one relationship between the entropies  $S_\alpha$  and the eigenenergies  $\mathcal{E}_\alpha$  of the many-body eigenstates.

The advantage of the dependence  $S(E)$  is related to the fact that both variables  $S$  and  $E$  are extensive variables, and thus their values have smaller fluctuations compared to probability distributions (12). This feature has been noted and used for nonlinear chains with disorder [31,32] and Bose-Einstein condensates, described by the Gross-Pitaevskii equation, in chaotic two-dimensional billiards [33]. It is interesting to note that in these nonlinear systems [31–33] the DTC is still valid but is induced by nonlinear mean-field interactions between linear states.

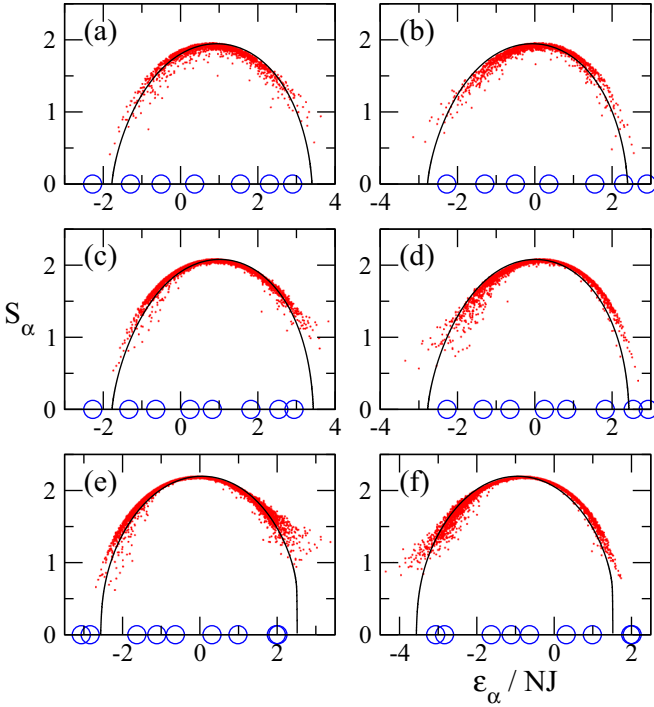


FIG. 4. Entropy per particle versus total energy per particle for the Bose-Hubbard ring (1) with on-site energies  $\epsilon_i$  that are randomly selected within  $-2J < \epsilon_i < 2J$ . The red dots show the entropies that are obtained from the many-body eigenstates according to Eq. (15) for the sizes [(a) and (b)]  $L = N = 7$ , [(c) and (d)]  $L = N = 8$ , and [(e) and (f)]  $L = N = 9$  and for the interaction strengths  $U = 0.5J$  (left) and  $U = -0.5J$  (right). They are plotted as a function of the associated eigenenergies  $\mathcal{E}_\alpha$  divided by the number of particles  $N$ . The solid lines show the entropies that are obtained from the Bose-Einstein distribution (12) according to Eq. (16) for all possible (positive and negative) temperatures as a function of the corresponding energies  $\bar{\epsilon}$  (18), using the single-particle eigenenergies  $E_k$  of the Bose-Hubbard system, which are displayed as blue circles on the abscissae.

The entropy of probability distribution (15) can also be obtained in the framework of the grand canonical ensemble described by the Bose-Einstein distribution (12). We obtain

$$\bar{S}(\beta, \mu) = - \sum_k \frac{\bar{n}_k(\beta, \mu)}{N(\beta, \mu)} \ln \left( \frac{\bar{n}_k(\beta, \mu)}{N(\beta, \mu)} \right), \quad (16)$$

with the total number of particles being given by

$$N(\beta, \mu) = \sum_k \bar{n}_k(\beta, \mu). \quad (17)$$

We can then calculate  $\bar{S}(\beta, \mu)$  for all possible (positive and negative) values of  $\beta$  where the chemical potential  $\mu$  is chosen such that the total population of the system according to Eq. (17) equals the total number of particles:  $N(\beta, \mu) = N$ . This population entropy can be plotted versus the effective energy per particle

$$\bar{\epsilon}(\beta, \mu) = \sum_k \frac{\bar{n}_k(\beta, \mu)}{N(\beta, \mu)} \tilde{E}_k = \sum_k \frac{\bar{n}_k(\beta, \mu)}{N(\beta, \mu)} E_k + NU/L \quad (18)$$

determined in analogy with Eq. (14), where we apply the mean-field shift (8) to account for the presence of the interaction.

The resulting curves are displayed by the solid lines in Fig. 4. We find a very good agreement with the population entropies  $S_\alpha$  obtained from the many-particle eigenstates  $|\phi_\alpha\rangle$  for both positive and negative interaction strengths  $U = \pm 0.5J$ . Significant deviations occur near the upper bound of the spectrum for positive interaction strengths and near the lower bound of the spectrum for negative interaction strengths. Indeed, many-body eigenstates in this regime are typically characterized by a rather strong localization of the population on a very small number  $\tilde{L} \ll L$  of Bose-Hubbard sites. The effective mean-field shift  $\bar{\epsilon} \mapsto \bar{\epsilon} + NU/\tilde{L}$  that one would have to apply in this regime is therefore much more important than elsewhere in the many-body spectrum.

As each point on the solid lines in Fig. 4 is characterized by a well-defined temperature, we are now in a position to determine the effective temperature  $T_\alpha$  associated with a many-body eigenstate  $|\phi_\alpha\rangle$  either from its energy per particle  $\mathcal{E}_\alpha/N$  or from its population entropy  $S_\alpha$ . Both possibilities

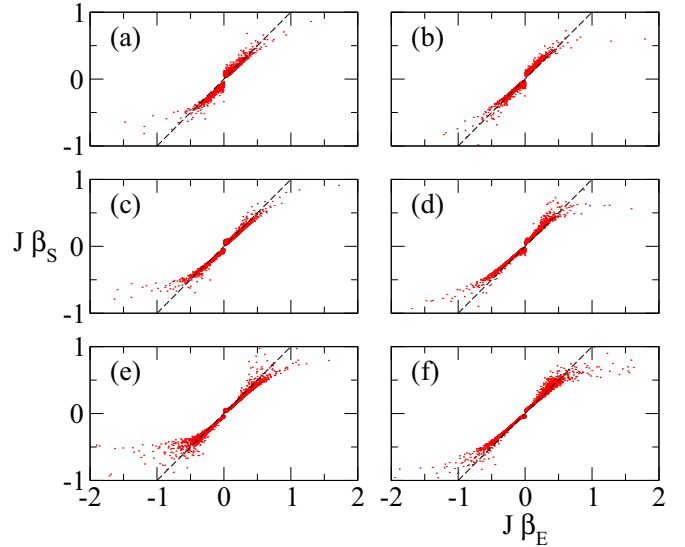


FIG. 5. Inverse temperatures  $\beta = 1/(k_B T)$  associated with the many-body eigenstates of the Bose-Hubbard ring for the sizes  $L = N = 7$  (top),  $L = N = 8$  (middle), and  $L = N = 9$  (bottom), for the interaction strengths  $U = 0.5J$  (left) and  $U = -0.5J$  (right), and for on-site energies  $\epsilon_i$  that are randomly selected within  $-2J < \epsilon_i < 2J$ , in perfect analogy with the panels shown in Fig. 4. The horizontal axis shows the inverse temperatures  $\beta_E$  that are obtained from intersecting the energy per particle  $\mathcal{E}_\alpha/N$  of the eigenstate under consideration with the corresponding entropy-versus-energy curve obtained from the Bose-Einstein distribution (solid lines in Fig. 4). The vertical axis shows the inverse temperatures  $\beta_S$  that are obtained from intersecting the population entropy (15) with the corresponding entropy-versus-energy curve. Both possible definitions of the effective temperature of a many-body eigenstate yield, on average, very similar values, as can be seen from the fact that all data points are scattered about the diagonal (indicated by dashed lines), with systematic deviations occurring in the regimes of low positive or negative temperatures to be encountered near the lower and upper bounds of the spectrum.

yield very similar temperatures, as is seen in Fig. 5. Systematic deviations between these two possible definitions of the temperature associated with a many-body eigenstate occur in the regimes of low positive or negative temperatures, which are to be encountered near the lower and upper bounds of the spectrum.

Calculating the arithmetic average of the two possible definitions of the temperature associated with a many-body eigenstate and plotting this average temperature as a function of the associated energy per particle and entropy yield very good agreement with the prediction obtained from the Bose-Einstein distribution (12), as is seen in Fig. 6. The same holds true for the chemical potential  $\mu$  of a many-body eigenstate, which can also be determined either from the corresponding energy per particle  $\mathcal{E}_\alpha/N$  or the corresponding population entropy  $S_\alpha$ . This underlines the validity of the DTC in the context of finite Bose-Hubbard systems.

Finally, we show in Fig. 7 that the reduced one-body density matrices associated with the many-body eigenstates  $|\Phi_\alpha\rangle$  are rather close to diagonal matrices. To this end, we plot in Fig. 7 the densities

$$p_{k,k'}^{(\alpha)} = |\langle \Phi_\alpha | \hat{b}_k^\dagger \hat{b}_{k'} | \Phi_\alpha \rangle / N|^2, \quad (19)$$

which correspond to the square moduli of the one-body density matrix elements  $\langle \Phi_\alpha | \hat{b}_k^\dagger \hat{b}_{k'} | \Phi_\alpha \rangle$  normalized by the number of particles. These densities are plotted both for individual many-body eigenstates (top row) and for averages of over 100 consecutive eigenstates in the many-body spectrum (bottom row of Fig. 7). The logarithmic grayscale plot clearly indicates that this one-body density matrix is very close to a diagonal matrix. This is precisely what one should expect to occur

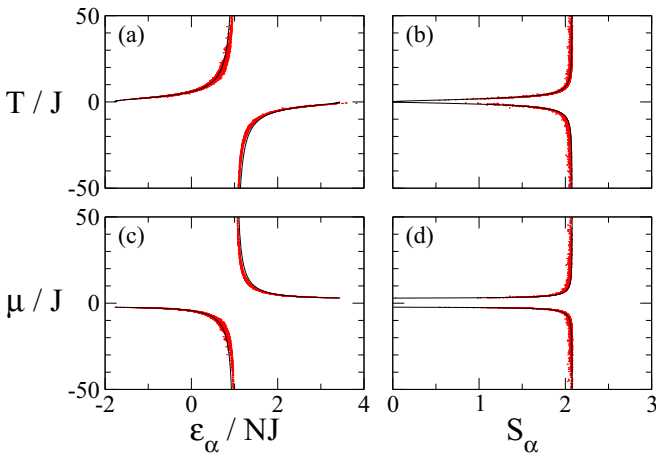


FIG. 6. [(a) and (b)] Average temperatures  $T$  and [(c) and (d)] chemical potentials  $\mu$  of the many-body eigenstates as a function of their energies per particle  $\mathcal{E}_\alpha/N$  (left) and their entropies  $S_\alpha$  (right) for the Bose-Hubbard ring with  $L = N = 8$ ,  $U = 0.5J$ , and on-site energies that are randomly selected within  $-2J < \epsilon_l < 2J$ . In (a) and (b), the red dots show the average temperatures  $(\beta_E^{-1} + \beta_S^{-1})/2$ , where  $\beta_E$  and  $\beta_S$  are taken from Fig. 5. The red dots in (c) and (d) show the average chemical potentials  $(\mu_E + \mu_S)/2$ , where  $\mu_E$  and  $\mu_S$  are obtained in a manner perfectly analogous to  $\beta_E$  and  $\beta_S$ , respectively. The solid lines display the corresponding predictions from the Bose-Einstein distribution (12).

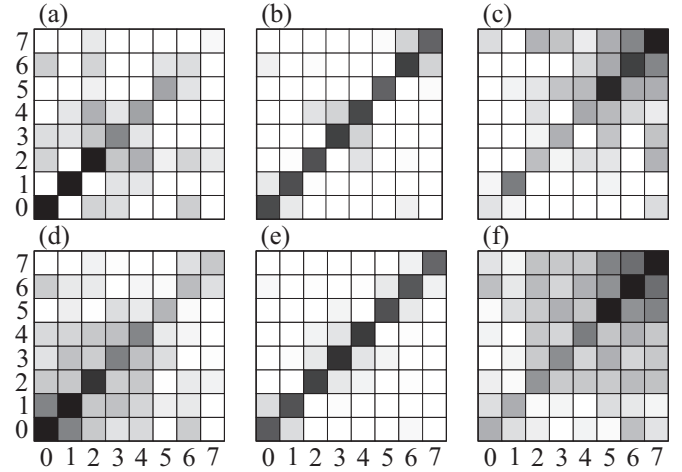


FIG. 7. One-body density matrix elements associated with various many-body eigenstates of the Bose-Hubbard ring with  $N = 8$  particles on  $L = 8$  sites and the interaction strength  $U = 0.5J$ . Top: On a logarithmic scale which uniformly varies from 1 (black) to  $10^{-5}$  (white), the densities  $p_{k,k'}^{(\alpha)}$  defined in Eq. (19) as a function of  $k$  and  $k'$  (on the horizontal and vertical axes, respectively) for the eigenstates (a)  $\alpha = 100$ , (b)  $\alpha = 3000$ , and (c)  $\alpha = 6300$ . Bottom: Average densities  $\bar{p}_{k,k'} = 0.01 \sum_{\alpha=\alpha_0-49}^{\alpha_0+50} p_{k,k'}^{(\alpha)}$  for (d)  $\alpha_0 = 100$ , (e)  $\alpha_0 = 3000$ , and (f)  $\alpha_0 = 6300$ .

in the framework of the grand canonical ensemble defined by Eq. (9).

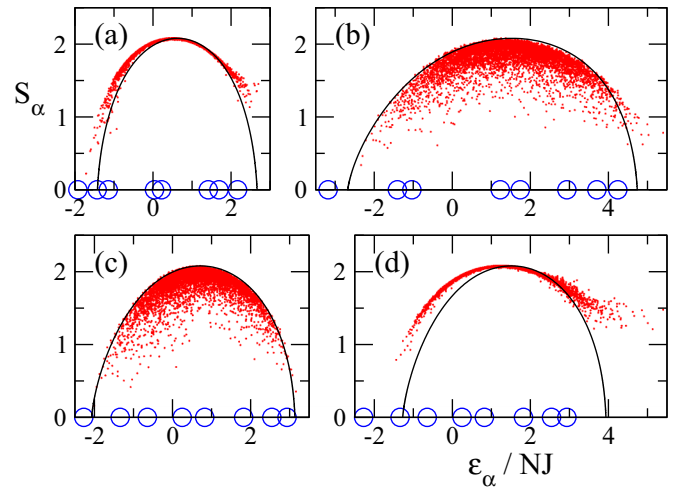


FIG. 8. Same as Fig. 4 for variable interaction and disorder strengths (a)  $U = 0.5J$ ,  $-0.5J < \epsilon_l < 0.5J$ , (b)  $U = 0.5J$ ,  $-4J < \epsilon_l < 4J$ , (c)  $U = 0.2J$ ,  $-2J < \epsilon_l < 2J$ , and (d)  $U = J$ ,  $-2J < \epsilon_l < 2J$  for the Bose-Hubbard ring (1) containing  $N = 8$  particles on  $L = 8$  sites. While the agreement with the DTC prediction is still very convincing for weak disorder in (a), a too low interaction strength  $U < U_c$  (see text) does not give rise to an efficient mixing of the noninteracting eigenstates of the system. This yields a number of interacting many-body eigenstates that are not fully thermalized, as is seen in (b) and (c). For a very strong interaction [in (d)], on the other hand, the considerations leading to the mean-field shift expression (8) are to be refined as the assumption of an equidistribution of the atoms within the lattice is expected to become invalid with increasing many-body eigenenergy.

It appears intuitively obvious that the occurrence of dynamical thermalization ought to be strongly linked to the validity of the ETH. Indeed, if the many-body eigenstates of the interacting quantum system are fully thermalized according to the ETH, we can formally derive the Bose-Einstein distribution for each single-particle eigenstate by treating this state as a “subsystem” that is coupled to a “reservoir” constituted by the other single-particle eigenstates. To support this link between the ETH and the DTC, we compare in Fig. 8 the numerically computed entropies of probability distribution (15) with the corresponding analytical prediction (16) for various values of the interaction and the disorder strength. As we clearly see in Figs. 8(b) and 8(c), dynamical thermalization becomes less effective if the interaction strength becomes smaller than a certain critical energy scale  $U_c$  below which the assumption of quantum ergodicity can no longer be taken for granted. According to the Åberg criterion [3,4,18,20], we would expect that this critical scale  $U_c$  be determined by comparing the interaction-induced matrix element between directly coupled noninteracting states with the energy level spacing between directly coupled states. Strictly speaking, however, this criterion does not apply to our system as we are not explicitly dealing with long-range interactions (and we cannot simply assume that all states be equally coupled with each other since the one-body localization length of the disordered system does not appear to exceed its size  $L$ ). Analogous computations for smaller systems with unit filling  $N = L < 8$  do, nevertheless, indicate that the DTC can be satisfied in the formal thermodynamic limit  $N = L \rightarrow \infty$  at weak (fixed) ratios  $U/J$ , in agreement with the mean-field studies undertaken in Ref. [34].

For very strong interactions, on the other hand, the considerations leading to the mean-field shift (8) would have to be refined, giving rise to a more involved expression for the shift that scales with the total energy per particle. Indeed, in the presence of a very strong interaction, we can safely assume that the ground state and the lowly excited eigenstates of the many-body system are characterized by an almost perfect equidistribution within the lattice, thereby minimizing the total interaction energy, while highly excited eigenstates in the center and close to the upper edge of the many-body spectrum are expected to exhibit a more and more peaked distribution of atoms on one or a few sites of the lattice. Correspondingly, the assumption of ergodicity is expected to break down with increasing interaction as individual Fock states defined with respect to the site basis become more and more isolated from each other and the system undergoes a transition to many-body localization. The situation simplifies again in the limit of ultrastrong interactions  $|U/J| \rightarrow \infty$ , where the system is approaching the case of noninteracting fermions (see, e.g., Ref. [35]).

#### IV. DISCUSSION

In this work we demonstrated that dynamical thermalization takes place for interacting bosons that are contained within a finite ring lattice exhibiting disordered on-site energies. While

the system is prepared in one of its many-body eigenstates, the atomic populations of the single-particle eigenstates of this disordered Bose-Hubbard system display the same thermalization features as they would if these single-particle eigenstates were coupled to an energy and particle reservoir according to the grand canonical ensemble. It is therefore possible to associate with each many-body eigenstate an effective temperature and an effective chemical potential. Evidently, the dynamical thermalization is caused by the presence of the atom-atom interaction, which should not be too weak to provide an effective mixing or so strong as to fully localize many-body eigenstates on restricted spatial regions within the lattice. In the regime of moderate interactions, individual eigenstates are well described by the Bose-Einstein thermal distribution satisfying DTC and ETH.

Dynamical thermalization may therefore provide a novel tool to probe the validity of ETH in an interacting many-body system, which appears all the more useful from an experimental point of view as it is solely based on the evaluation of one-body observables, namely, the populations of single-particle eigenstates. In practice, these populations can be inferred from the single-site occupations of the lattice whose measurement was pioneered in Ref. [36] and from the corresponding off-diagonal coherences (i.e., from the reduced one-body density matrix of the system in the site representation), as well as from precise knowledge of the involved intersite hopping and on-site energies of the lattice. Conversely, the assumption of eigenstate thermalization allows us now to theoretically predict the single-particle eigenstate populations within a many-body eigenstate of the system *without doing any numerical many-body computation*: all we need to know for this purpose is the relative location of the energy per particle of this many-body eigenstate within the single-particle eigenspectrum, as well as the on-site interaction strength in order to correctly account for the effective mean-field shift (8) of the single-particle energies.

Restricting ourselves to finite size systems with up to nine bosons, we do not analyze in this work the conditions of validity of the DTC in this Bose-Hubbard system. The determination of the conditions under which the DTC is valid is a much more involved task which is beyond the scope of this paper. In the case of long-range interactions we expect that the Åberg criterion will work well as it was the case for fermionic [18] and qubit systems [19,20]. In the case of a finite interaction range, however, the noninteracting eigenstates can be localized, and the validity of the DTC can depend on the system size, on the nature and strength of interactions, and on the disorder strength. The investigation of DTC and ETH in systems with a finite interaction range is now attracting growing interest with the possible appearance of phase transitions (see, e.g., Ref. [37] and references therein). We expect that experimental tests of the DTC with cold atoms will allow us to investigate this fundamental problem in great detail.

#### ACKNOWLEDGMENTS

We thank D. Delande and J. D. Urbina for useful discussions and suggestions.

- [1] L. D. Landau and E. M. Lifshitz, *Statistical Physics* (Nauka, Moscow, 1976) [in Russian].
- [2] N. Bohr, *Nature (London)* **137**, 344 (1936).
- [3] S. Åberg, *Phys. Rev. Lett.* **64**, 3119 (1990).
- [4] S. Åberg, *Prog. Part. Nucl. Phys.* **28**, 11 (1992).
- [5] J. M. Deutsch, *Phys. Rev. A* **43**, 2046 (1991).
- [6] M. Srednicki, *Phys. Rev. E* **50**, 888 (1994); *J. Phys. A* **29**, L75 (1996); **32**, 1163 (1999).
- [7] R. Fratus and M. Srednicki, *Phys. Rev. E* **92**, 040103(R) (2015).
- [8] L. D'Alessio, Y. Kafri, A. Polkovnikov, and M. Rigol [arXiv:1509.06411](https://arxiv.org/abs/1509.06411) [Advances in Physics (to be published)].
- [9] A. I. Shnirelman, *Usp. Mat. Nauk* **29**, 181 (1974).
- [10] I. P. Cornfeld, S. V. Fomin, and Y. G. Sinai, *Ergodic Theory* (Springer, New York, 1982).
- [11] O. Bohigas, M. J. Giannoni, and C. Schmit, *Phys. Rev. Lett.* **52**, 1 (1984).
- [12] L. E. Reichl, *The Transition to Chaos: Conservative Classical Systems and Quantum Manifestations* (Springer, New York, 2004).
- [13] F. Haake, *Quantum Signatures of Chaos* (Springer, Berlin, 2010).
- [14] E. Wigner, *Ann. Math.* **62**, 548 (1955); **65**, 203 (1957).
- [15] A. Bohr and B. R. Mottelson, *Nuclear Structure* (Benjamin, New York, 1969), Vol. 1.
- [16] T. Guhr, A. Müller-Goelting, and H. A. Weidenmüller, *Phys. Rep.* **299**, 189 (1998).
- [17] D. L. Shepelyansky and O. P. Sushkov, *Europhys. Lett.* **37**, 121 (1997).
- [18] P. Jacquod and D. L. Shepelyansky, *Phys. Rev. Lett.* **79**, 1837 (1997).
- [19] B. Georgeot and D. L. Shepelyansky, *Phys. Rev. E* **62**, 6366 (2000).
- [20] G. Benenti, G. Casati, and D. L. Shepelyansky, *Eur. Phys. J. D* **17**, 265 (2001).
- [21] D. L. Shepelyansky, *Phys. Scr.* **T90**, 112 (2001).
- [22] B. V. Chirikov, *Phys. Lett. A* **108**, 68 (1985).
- [23] V. V. Flambaum, A. A. Gribakina, G. F. Gribakin, and I. V. Ponomarev, *Phys. D (Amsterdam, Neth.)* **131**, 205 (1999).
- [24] M. Rigol, V. Dunjko, and M. Olshanii, *Nature (London)* **452**, 854 (2008).
- [25] T. Langen, S. Erne, R. Geiger, B. Rauer, T. Schweigler, M. Kuhnert, W. Rohringer, I. E. Mazets, T. Gasenzer, and J. Schmiedmayer, *Science* **348**, 207 (2015).
- [26] S. Braun, J. P. Ronzheimer, M. Schreiber, S. S. Hodgman, T. Rom, I. Bloch, and U. Schneider, *Science* **339**, 52 (2013).
- [27] M. Schreiber, S. S. Hodgman, P. Bordia, H. Lüschen, M. H. Fischer, R. Vosk, E. Altman, U. Schneider, and I. Bloch, *Science* **349**, 842 (2015).
- [28] T. Engl, J. Dujardin, A. Argüelles, P. Schlagheck, K. Richter, and J. D. Urbina, *Phys. Rev. Lett.* **112**, 140403 (2014).
- [29] A. Abragam, *The Principles of Nuclear Magnetism* (Oxford University Press, Oxford, 1961).
- [30] S. Bera, H. Schomerus, F. Heidrich-Meisner, and J. H. Bardarson, *Phys. Rev. Lett.* **115**, 046603 (2015).
- [31] M. Mulansky, K. Ahnert, A. Pikovsky, and D. L. Shepelyansky, *Phys. Rev. E* **80**, 056212 (2009).
- [32] L. Ermann and D. L. Shepelyansky, *New J. Phys.* **15**, 123004 (2013).
- [33] L. Ermann, E. Vergini, and D. L. Shepelyansky, *Europhys. Lett.* **111**, 50009 (2015).
- [34] G. Jona-Lasinio and C. Presilla, *Phys. Rev. Lett.* **77**, 4322 (1996).
- [35] I. V. Ponomarev and P. G. Silvestrov, *Phys. Rev. B* **56**, 3742 (1997).
- [36] W. Bakr, J. Gillen, A. Peng, S. Fölling, and M. Greiner, *Nature (London)* **462**, 74 (2009); J. Sherson, C. Weitenberg, M. Endres, M. Cheneau, I. Bloch, and S. Kuhr, *ibid.* **467**, 68 (2010).
- [37] D. J. Luitz, N. Laflorencie, and F. Alet, *Phys. Rev. B* **91**, 081103(R) (2015).